Improved Optical Instrument for the Measurement of Water Wave Statistics in the Field

Daniel Kiefhaber[1,2], Roland Rocholz[1], Günther Balschbach[1], and Bernd Jähne[1,2]

[1] *Institute of Environmental Physics, University of Heidelberg, Im Neuenheimer Feld 229, 69120 Heidelberg, Germany*

[2] *Heidelberg Collaboratory for Image Processing (HCI) at the Interdisciplinary Center for Scientific Computing, University of Heidelberg, Speyerer Straße 6, Heidelberg, Germany, E-mail: {daniel.kiefhaber, roland.rocholz, bernd.jaehneg}@iwr.uni-heidelberg.de*

Abstract. An improved optical instrument for the measurement of slope and height statistics of capillary and short gravity wind waves on the ocean has been built. This reflective stereo slope gauge (RSSG) is based on the work of Waas and Jähne (1992). It uses a dedicated stereo camera setup with a stereo infrared LED light source. Wave slope statistics can be derived from the observation of specular reflections and wave height from the parallax of the specular reflections in the stereo images. The instrument has been successfully tested in the Heidelberg *Aeolotron*.

Key Words: Wave slope statistics, optical instrument, specular reflections

1. Introduction

Gas exchange at the air-water interface is heavily dependent on the "shape" of the wave field. Numerous instruments and methods have been developed to measure properties of the wave field on the open ocean, ranging from capacitance wires to satellite-born radar. Optical methods have the advantage of being nonintrusive, eliminating interaction of the instrument with the wave field. Cox and Munk (1954b), the pioneers of optical wave statistics measurements, took photographs of reflections of the sun ("sun glitter") on the sea surface and derived slope probability distributions (Cox and Munk, 1954a).

Another, more recent, approach of reflection-based measurements of the water surface structure by Zappa *et al*. (2008) is using the angular dependence of the polarization of reflected light. This *polarimetric imaging* technique is able to reconstruct dense 2D slope maps of the water surface, but is limited to restricted environmental conditions with diffuse skylight.

Based on the work of Cox and Munk, Waas and Jähne (1992) developed the reflective stereo slope gauge (RSSG). By using artificial light sources, the RSSG can measure surface slope statistics independent of daytime and environmental

conditions. A special stereo camera setup that is optimized for the specularly reflecting water surfaces, allows the simultaneous measurement of wave amplitudes. In this work, a modified and improved RSSG is presented. It is intended to measure local wave slope statistics during gas or heat transfer experiments, e.g. with the active controlled flux technique (ACFT) by Schimpf *et al*. (2010).

The RSSG measurement method is explained in section 2, the field measurement instrument is described in section 3. In section 4, two algorithms to determine the mean square slope of the water surface from the RSSG images are detailed, while in section 5, first results from laboratory test measurements are presented.

2. Method

The reflective stereo slope gauge (RSSG) combines the measurement of wave slope from the statistical distribution of specular reflections on the water surface with the measurement of wave height from stereo triangulation.

The slope measurement is based on the Cox and Munk sun glitter method, but is using an artificial light source to eliminate the need for daytime and clear sky during measurements. The statistical distribution of reflections in the RSSG images is proportional to the slope probability distribution for small slopes in the range of $-0.08 < s < 0.08$ and statistical parameters such as the mean square slope can be extrapolated from this data.

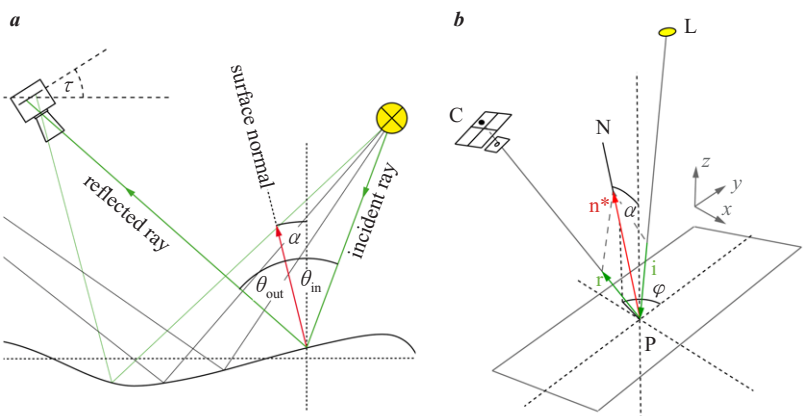

Figure 1 **a** The RSSG slope measurement principle: If light rays are reflected into the camera, the surface slope $s = \tan \alpha$ can be determined from geometric considerations and the reflection condition $\theta_{in} = \theta_{out}$. **b** The RSSG geometry of reflection: An incident ray coming from the light source L is reflected at the point P on the water surface into the camera at C.

The wave height measurement by stereo triangulation requires a setup of two cameras which are observing the water surface from different perspectives. As will be described in section 2.2, the specular nature of reflections at the water surface additionally requires the use of two light sources in dedicated positions.

2.1 Slope Measurement

Figure 1a illustrates the slope measurement principle. For light rays coming from the light source to enter the camera aperture, the water surface normal vector **n** needs to be tilted in the direction determined by the condition for specular reflection, i.e. the incident angle θ_{in} (between the light ray and the surface normal) equals the reflected angle θ_{out}. Thus, the surface normal $\mathbf{n}^* = \hat{\mathbf{r}} - \hat{\mathbf{i}}$, where $\hat{\mathbf{i}}$ and $\hat{\mathbf{r}}$ are the vectors of unit length in the direction of the incident and reflected beam, respectively (see Figure 1b). For a camera at position **c** to observe a reflection at position **x** on the water surface, with the reflected light beam coming from a light source at position **l**, the surface normal needs to satisfy the condition

$$\mathbf{n}^* = \hat{\mathbf{r}} - \hat{\mathbf{i}} = \frac{\mathbf{r}}{|\mathbf{r}|} - \frac{\mathbf{i}}{|\mathbf{i}|} = \frac{\mathbf{c}-\mathbf{x}}{|\mathbf{c}-\mathbf{x}|} - \frac{\mathbf{x}-\mathbf{l}}{|\mathbf{x}-\mathbf{l}|}. \tag{1}$$

In a world coordinate system with the z-axis pointing vertically upwards the slope components $s_x = \partial\eta/\partial x$ and $s_y = \partial\eta/\partial y$ are given by the x- and y-component of $\mathbf{n}^*/n_z^*$. Here, η is the surface elevation.

In a camera coordinate system with the z-axis pointing along the optical axis, the position $\mathbf{x}_c$ of the reflecting water surface patches in Eq. (1) is related to the image (pixel) coordinates u and v

$$\mathbf{x}_c = \begin{pmatrix} z_c u/f \\ z_c v/f \\ z_c \end{pmatrix}, \tag{2}$$

where f is the focal length and $\mathbf{x}_c$ is the vector between the surface patch and the aperture of the camera. The distance z_c is measured by stereo triangulation, see section 2.2.

During field experiments, the relative orientation of the camera coordinate system to the world coordinate system changes in time due to pitch and roll of the vessel carrying the RSSG. The transformation of the surface normal $\mathbf{n}_c^*$, determined with Eq. (1) given in the camera coordinate system into the surface normal $\mathbf{n}^*$ in the world coordinate system can be formally written as

$$\mathbf{n}^* = \mathbf{P}(\psi)\mathbf{R}(\rho)\mathbf{C}^{-1}(\tau)\mathbf{n}_c^*, \tag{3}$$

where $\mathbf{P}(\psi)$ and $\mathbf{R}(\rho)$ are rotation matrices accounting for pitch ψ and roll ρ, and

$\mathbf{C}^{-1}(\tau)$ is accounting for the tilt of the optical axis. Pitch and roll are measured by an inclination sensor, τ is defined by the fixed stereo setup.

Combining Eq. (1) and Eq. (3) yields the desired relation of image coordinates $[u, v]$ and the water surface slope $[s_x, s_y]$ at specular reflections (Kiefhaber, 2010). The exact result is lengthy due to the normalization factors, but the relation is linear to a good approximation as can be seen from the plot of s_x versus pixel position u for different values of z_c that is shown in Figure 2.

2.2 Height Measurement

The distance of the camera to the water surface z_c is measured by stereo triangulation. The relative shift (the parallax) of the specular reflections in the images of two cameras observing the water surface from different perspectives is uniquely related to the water surface distance, see Figure 3a. The distance between the two cameras is the stereo base b. Their optical axes are tilted against each other, enclosing angles of τ and $-\tau$ with the vertical, to ensure maximum overlap of the image footprints. The distance at which the optical axes of the cameras intersect is referred to as the stereo reference height Z_0. In Figure 3b the parallax dependence on water surface distance is plotted for the RSSG setup with the stereo base $b=300$mm and the reference height $Z_0=6000$mm.

To solve the *correspondence problem* of stereo vision, i.e. to find corresponding reflections in both images to relate their parallax to water surface distance at the specular water surface, it is required that the reflections in the stereo images are coming from the same spots on the water surface. This can be guaranteed if the second camera is virtually placed at the position of the light source, while a second light source is placed at the position of the first camera.

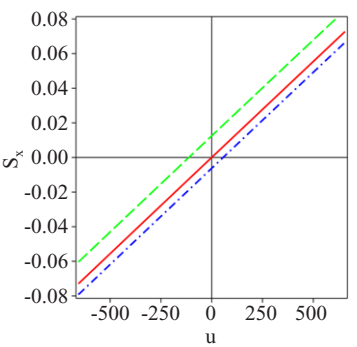

Figure 2 Dependence of the measured slope component s_x on image pixel position u for water surface distances $Z=4$m (solid), $Z=6$m (dashed), and $Z=8$m (dashdot). Used parameters: $b=300$mm, $Z_0=6$ m.

Then, the paths of reflected light rays into the cameras are identical, their directions opposite. Stereo triangulation only needs the parallax in the direction parallel to the stereo base, thus it is sufficient to require for the light source to be placed at the position of the aperture *in this direction*. This allows the use of a light source which is extended in a direction orthogonal to the stereo base next to the camera (see Figure 4).

3. Instrument

The RSSG field instrument is shown in Figure 4a. The image acquisition system comprises two cameras and two light sources. The light sources are extended in the direction orthogonal to the stereo base to provide sufficient illumination even at higher wind speeds when the water surface is roughened. If the patches that fulfill the reflection condition on the surface are smaller than the projection of a single pixel, the reflected intensity is decreased and the reflection can hardly be separated from background noise. Thus, it is necessary to weaken the reflection condition by extending the light source (Kiefhaber, 2010). The light sources are built from infrared light emitting diodes (LEDs) with a centroid wavelength of 950 nm. This wavelength is close to a major water absorption peak, thus the penetration depth of the light in water is only 3.4 cm. This is necessary since less than 2% of the light are reflected at the surface, and the light that is transmitted through the water surface could be reflected by particles in the water. This upwelling light would cause false stereo correspondences and errors in the

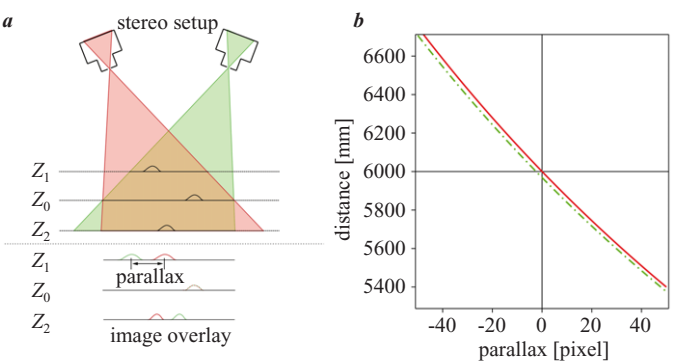

Figure 3 **a** The origin of stereo parallax: An object at the reference distance Z_0 is projected onto the same image coordinates in both images. For smaller (Z_1) or greater (Z_2) distances, image coordinates are shifted, the parallax is the relative shift in the overlay image. **b** The dependence of parallax on distance for the image center ($u=0$, solid line) and a pixel at the image border ($u=656$, dashed line). Used parameters: $f=72$mm, $b=300$mm, $Z_0=6000$ mm.

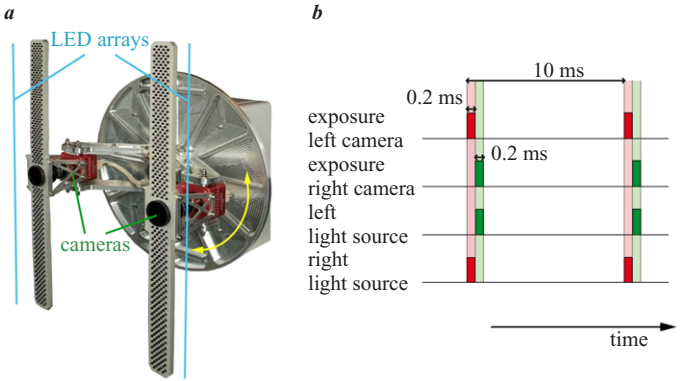

Figure 4 **a** The setup that is used for field experiments. The stereo base length is 300 mm, the light sources are LED arrays built from 350 IR-LEDs each. The image acquisition system consisting of cameras and light sources can be rotated about the center of the stereo base. **b** The trigger scheme used in image acquisition. Left camera and right light source are synchronized, and vice versa.

slope distributions and thus needs to be suppressed.

As was noted in section 2, the measurement method requires that each camera only sees the opposite light source. In the RSSG, this is achieved by sequential image acquisition. Figure 4b shows the triggering scheme that is used. The LED arrays are pulsed so that the exposure of the left camera coincides with a flash of the right light source and vice versa. The delay in the acquisition of the second image is 0.2 ms.

LEDs provide high and efficient power output with a relatively narrow spectrum. However, the asymmetry and inhomogeneity of the directional radiation characteristic distorts the slope probability distribution (Kiefhaber 2010). In the RSSG field instrument, holographic diffusors are placed in front of the LEDs to homogenize the emitted light.

4. Data Evaluation

Two different methods are used for the computation of the mean square slope from speckle images. The first one only uses the mean gray value of the image portion around slope zero, while the second fits a simplified convoluted slope PDF to the data in the whole slope range.

According to Cox and Munk (1954a) and Bréon and Henriot (2006), the slope PDF can be described by a truncated Gram-Charlier series. This Gram-Charlier series is essentially Gaussian with added higher order skewness and peakedness terms. The skewness leads to a shift of the maximum as well as an asymmetry of

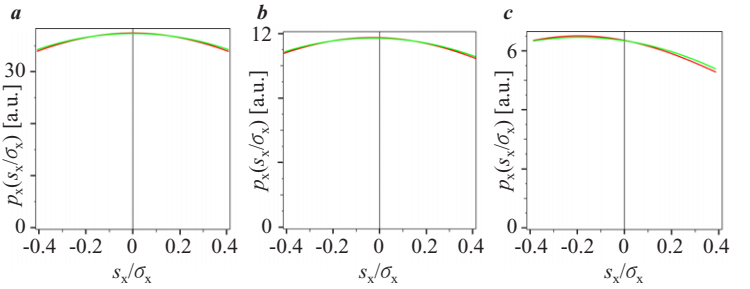

Figure 5 Comparison of the Cox/Munk Gram-Charlier expansion (up-/ downwind direction, *dark gray*) and the approximation in Eq. (4) (*light gray*) for wind speeds **a** 1 m/s, **b** 5 m/s, and **c** 10 m/s.

the distribution. The peakedness leads to increased probabilities for small and large slopes. The RSSG acquires data corresponding to very small slopes only. In this range, the Gaussian can be approximated by a parabola. The peakedness can be approximated by a constant factor and skewness is modeled by allowing a shift of the maximum of the parabola $s_{x,0}$. The simplified PDF then becomes:

$$p(s_x, s_y) = \frac{1}{2\pi\sigma_x\sigma_y}\left(1 - \frac{(s_x - s_{x,0})^2}{2\sigma_x^2} - \frac{s_y^2}{2\sigma_y^2}\right). \tag{4}$$

In Figure 5, the approximated PDF is compared to the Cox and Munk Gram-Charlier distribution, in the slope range that is visible to the RSSG. The agreement is acceptable, however, some deviations occur: At very low wind speeds, σ_x and σ_y are small, the assumptions $s_x \ll \sigma_x$ and $s_y \ll \sigma_y$ are no longer valid for the image borders and deviations of the approximated PDF increase. At higher wind speeds ($U_{10} \geq 10$m/s), the influence of skewness increases and the fit quality decreases.

4.1 Mean Gray Value

The brightness distribution in the speckle images is proportional to the slope PDF in Eq. (4) after a convolution with a function describing the expansion of the LED arrays. Integrating this brightness distribution function (which is equivalent to computing the mean gray value G), yields

$$G = \frac{2\delta s_x \delta s_y \Delta s_x \Delta s_y}{\pi\sigma_x\sigma_y}\left(1 - \frac{s_{x,0}^2}{2\sigma_x^2} - \frac{\delta s_x^2}{6\sigma_x^2} - \frac{\delta s_y^2}{6\sigma_y^2}\right), \tag{5}$$

where $\delta s_{x/y}$ denotes the dimension of the light sources and $\Delta s_{x/y}$ is the size of the integration interval, i.e. the area of the image used in computing the mean gray value. If all but the first of the terms in the brackets can be neglected, then $G \propto \frac{1}{\sigma_x\sigma_y}$ from which the mean square slope can be estimated. The third and fourth

term in Eq. (5) are consequences of the finite size of the light source. As long as $\delta s_{x/y}^2 \ll 6\sigma_{x/y}^2$, they can be neglected. In the critical y-direction, $\delta s_y = 0.017$. Even at near zero wind speed, rms slope is of the order $\sigma_{x/y} \approx 0.03$ (Cox and Munk 1954a; Bréon and Henriot 2006), thus the approximation is reasonable and the error introduced by neglecting the term is expected to be small. The dimension of the light source in the x-direction is negligible. The second term in Eq. (5) is a consequence of the non-linear wave-wave interaction and the skewness[1] of the slope PDF. At low wind speeds, the shift of the maximum due to distribution peakedness that is modeled with $s_{x,0}$ is near zero and experimentally it is found that $s_{x,0}$ increases slower than σ_x, therefore $s_{x,0}^2$ is negligible to a good approximation (Bréon and Henriot 2006).

Under these approximations, the mean gray value of the image is proportional to the product of the root mean square (rms) slope components $G \propto \frac{1}{\sigma_x \sigma_y}$. Writing $\epsilon := \frac{\sigma_x}{\sigma_y}$, the mean square slope is obtained from the rms component product using

$$\sigma_x \sigma_y = \frac{1}{\epsilon}\sigma_x^2 \quad \text{and} \quad \sigma_x \sigma_y = \epsilon \sigma_y^2, \tag{6}$$

so that the total mean square slope is

$$\sigma^2 = \sigma_x^2 + \sigma_y^2 = \left(\epsilon + \frac{1}{\epsilon}\right)\sigma_x \sigma_y \propto \frac{\epsilon + 1/\epsilon}{G}. \tag{7}$$

From the analysis of experimental data of measurements by Cox and Munk (1954a) and Bréon and Henriot (2006) it is found that the value of $\epsilon + 1/\epsilon$ is almost independent of wind speed (Kiefhaber, 2010). Thus to a good approximation σ^2 is proportional to $1/G$.

4.2 Parabolic Fit

The integration of the gray value of the image in the y-direction gives (Kiefhaber, 2010):

$$p_x(s_x) = -\frac{\delta s_x \delta s_y \Delta s_y}{\pi \sigma_x^3 \sigma_y}(s_x - s_{x,0})^2 + \frac{2\delta s_x \delta s_y \Delta s_y}{\pi \sigma_x \sigma_y}\left(1 - \frac{\delta s_x^2}{2\sigma_x^2} - \frac{\delta s_y^2}{2\sigma_y^2}\right), \tag{8}$$

By fitting a parabola of the form $a_0(x - x_0)^2 + a_1$ to this distribution, the parameters a_0 and a_1 can be used to extract both rms slope components and thus the mean square slope:

1 The skewness is only modeled with this shift of the maximum, since the approximated PDF used here is symmetric about its maximum.

$$a_0 = -\frac{\delta s_x \delta s_y \Delta s_y}{\pi} \frac{1}{\sigma_x^3 \sigma_y}, \quad a_1 = \frac{2\delta s_x \delta s_y \Delta s_y}{\pi \sigma_x \sigma_y} \left(1 - \frac{\delta s_x^2}{2\sigma_x^2} - \frac{\delta s_y^2}{2\sigma_y^2}\right). \tag{9}$$

This (nonlinear) equation system can be solved numerically to directly yield σ_x and σ_y without the need of further assumptions (Kiefhaber, 2010).

Note that it is critical for this approach that the gray value distribution in the image depends only on reflection probability. This requires that the illumination is homogeneous and vignetting does not occur. Furthermore, using this method, the values for σ_x and σ_y rely heavily on the extrapolation of the PDF to higher slope values and are not directly computed from measurement data.

5. First Results

Figure 7 shows sample images acquired during the July 2010 field campaign in the Baltic Sea. A precursor laboratory version of the RSSG with smaller light sources was installed at the Heidelberg *Aeolotron* circular wind wave facility. Simultaneous measurements of wave slope statistics were performed by both the RSSG and a color imaging slope gauge (CISG) (Rocholz, 2008). The mean square slope (mss or σ^2) was extracted from the RSSG data by the mean gray value method. The method was chosen because of the limited field of view in the lab setup, only slopes in the range of −0.06 to 0.06 were visible. Figure 6 compares the results of the CISG and RSSG mss measurements, plotted against a reference wind speed. There is qualitative agreement, the mss increases linearly with a change in slope around 3.5 m/s, this coincides with first micro-breaking of the short gravity waves.

At higher wind speeds however, the RSSG overestimates the mss. This overestimation of the mss is caused by an underestimation of the gray values in the

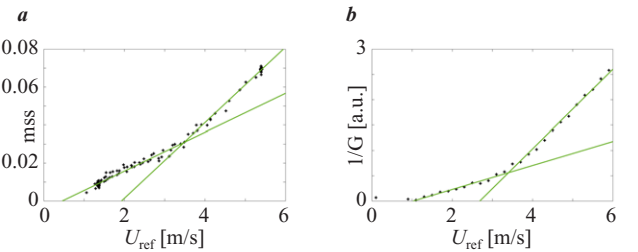

Figure 6 **a** The dependence of the mean square slope on wind speed, measured with the CISG. **b** The dependence of the factor $1/G$, determined from RSSG data, on wind speed. The factor is proportional to the mean square slope, according to Eq. (7). Measurements were conducted at the Heidelberg *Aeolotron* wind-wave facility.

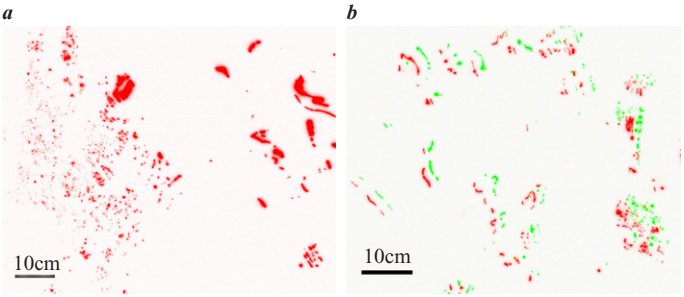

Figure 7 **a** Detail of speckle image acquired with the RSSG. In the right part, a surfactant smoothens the water surface, the speckle intensity and size is increased, while the number of speckles is decreased. **b** Overlay of left (red) and right (green) stereo images. Deviations in speckle size and shape are due to different sizes of the left and right light sources used for this image.

images. One reason for this underestimation is a faulty segmentation algorithm that was used in data preprocessing. This algorithm was intended to reduce data size but as a matter of fact "cut out" a significant number of reflections that had a brightness of the order of the background noise level. In the field instrument, this algorithm is not used. In addition, the light source size was quadrupled to ensure sufficient illumination even at high wind speeds.

6. Outlook

It is desired to cross-validate the RSSG data with data acquired by other instruments to determine the proportionality factor in Eq. (7). Furthermore, an efficient stereo evaluation algorithm that is expected to allow the reconstruction of the height of the longer waves is currently under development.

References

Bréon, F. M. and N. Henriot (2006), Spaceborne observations of ocean glint reectance and modeling of wave slope distributions, *J. Geophys. Res. (Oceans), 111,* 6005-+.

Cox, C. and W. Munk (1954a), Measurements of the roughness of the sea surface from photographs of the sun's glitter, *J. Opt. Soc. Amer., 44* (11), 838-850.

Cox, C. and W. Munk (1954b), Statistics of the sea surface derived from sun glitter, *J. Mar. Res., 13* (2), 198-227.

Kiefhaber, D. (2010), *Development of a Reective Stereo Slope Gauge for the Measure- ment of Ocean Surface Wave Slope Statistics*, Diploma thesis, Institut für Umweltphysik, Fakultät für Physik und Astronomie, Univ. Heidelberg.

Rocholz, R. (2008), *Spatiotemporal Measurement of Short Wind-Driven Water Waves*, Dissertation, Institut für Umweltphysik, Fakultät für Physik und Astronomie, Univ.

Heidelberg.

Schimpf, U., L. Nagel, and B. Jähne (2010), First results of the 2009 sopran active thermography pilot experiment in the baltic sea, *this volume*.

Waas, S. and B. Jähne (1992), Combined slope-height measurements of short wind waves: first results from field and laboratory measurements, in L. Estep (Ed.), *Optics of the Air-Sea Interface: Theory and Measurements, SPIE Proc*., vol. 1749, pp. 295-306.

Zappa, C., M. Banner, H. Schultz, A. Corrada-Emmanuel, L. Wolff, and J. Yalcin (2008), Retrieval of short ocean wave slope using polarimetric imaging, *Meas. Sci. Technol., 19*, 055503 (13pp).